Macula Precise Localization Using Digital Retinal Angiographies

C.MARIÑO, S. PENA, M.G.PENEDO, M. ORTEGA, J. ROUCO, †A. POSE-REINO, †M. PENA
Grupo de Visión Artificial y Reconocimiento de Patrones
University of A Coruña
Campus de Elviña s/n, A Coruña, 15071
†Service of Internal Medicine, Hospital de Conxo
†Santiago de Compostela, 15782
SPAIN
{castormp,mgpenedo,mortega,jrouco}@udc.es,antoniopose@telefonica.net,mpenaseijo@gmail.com

Abstract: The fovea is a spot located in the center of the macula, and responsible for sharp central vision. In this paper a method to detect the macula location and size is presented, as a first step towards the fovea location. Prior to the macula detection, the optic disk size and position is computed. This is performed through the combination of two stages: firstly, a clustering algorithm is used to select the regions which contain the pixels with the highest gray levels. A correlation filter is applied to these regions to compute the approximate center of the optic disk. Then, in order to extract the optic disk, a deformable model which is used. Then, following the morphological properties of the eye, the macula location and size is determined by means of a new correlation filter. Search with this filter is performed in a reduced area of interest, whose size and position is determined by means, again, of the morphological properties of the eye. The algorithm has proven to be fast and accurate in the set of test images, composed by 135 digital retinal images, where the tests have been performed by comparing our results with those obtained by two expert clinicians from two different hospital centers.

Key–Words: Optic disk, macula, fovea, correlation filter, deformable model.

1 Introduction

The retinal fundus photographs are widely used in the diagnosis of eye diseases. Processing automatically a large number of retinal images can help ophthalmologists to increase the efficiency in medical environment. The optic disk is the brightest area in images that have not large areas of exudates and it is a slightly oval disk. It is the entrance region of vessels and its detection is very important since it works as a landmark for the other features in the retinal image. The macula is a commonly visible as a hazy dark area. This is the area with the highest number of cones and rods per unit area.

There are many previous works on optic disk localization. Goldbaum et al. [1] extract the main features of the eye fundus (optic disk, vessels, blobs and fovea), through the combination of several templates, which work separately on the image color channels. Pinz et al. [2] also obtain a map of the human retina using retinal angiographies, obtaining very good results. Lalonde et al. [3] extract the optic disk using Hausdorff based template matching and pyramidal decomposition. It is neither sufficiently sensitive nor specific enough for clinical application. On the other hand, strategies based on active contours [4–6] are used to detect the optic disk boundary in retinal images. These techniques are very robust against noise but their main disadvantage is their high computational cost.

A method for the detection of the macular center was presented by Sinthanayothin [7]. In this approach a template based algorithm was used, combined with the morphological properties of the eye. The system showed an accuracy 80.4% on 100 images. Li et al. [8] presented a model based approach in which an snake was used to extract the vascular tree based on the location of the optic disk. Then, the information from the snake was used to find the macula center. The authors reported an accuracy 100% for optic disk localization and 100% for macula localization in 89 digital retinal images.

This paper presents an algorithm for the automatic localization and segmentation of the optic nerve head, macula and fovea working on digital retinal images. Without user intervention, the optic nerve head is located and its shape is extracted. Localization is achieved by means of a two stages algorithm: the former locates several regions of interest candidates , where the optic disk could be located. In the latter the regions where the optic disk is not present are rejected by means of a simple correlation filter. Once the optic disk position has been achieved, macula and fovea are

located using the morphological properties of the eye, combined with a correlation filter for a more accurate result.

The setup of the paper is as follows. In section 2 the algorithm for the optic disk localization, while section 3 provides details on the segmentation process. Section 4 describes the macula segmentation process. Experiments and results are given in section 5 for both the optic disk and macula localization and segmentation, and finally section 6 provides discussion and conclusions.

2 Optic Disk Localization

The first stage of the process consists of locating the region where the optic disk is located. A clustering algorithm is used to compute the regions with highest gray level pixels, among which will be the one containing the optic disk. Later, a correlation filter is applied to these regions in order to discard the regions where the optic disk is not located, and to compute the approximate center of the optic disk in the right region. With the addition of the clustering algorithm to the whole process proposed by Lowell et all. a better performance has been obtained, improving results by reducing the wrong localization cases, as will be shown in results chapter.

2.1 A Clustering Algorithm

Since the intensity of the optic disk is much higher than the retinal background, a possible method in order to localize the optic disk is to find the largest clusters of pixels with the highest gray levels. For this reason, the pixels with the highest 1% gray levels are selected. After this, a clustering algorithm groups the nearby pixels into clusters. Initially, each point is a cluster and its own centroid.If the Euclidean distance between two centroids is less than a specified threshold ε, these clusters are combined to form a new one. The new centroid (c_x, c_y) is computed by means of Equations 1 and 2.

$$c_x = \sum_{i=0}^{n} \frac{x_i}{n} \quad (1)$$

$$c_y = \sum_{i=0}^{n} \frac{y_i}{n} \quad (2)$$

where (x_i, y_i) are the cluster points and n is the number of points in the cluster.

If there are bright areas as well as the optic disk in the retinal image, the algorithm might compute several clusters. The regions of interest are defined as $n \times m$ rectangles whose centers are the centroids of these clusters. The rectangle size depends on the image resolution.

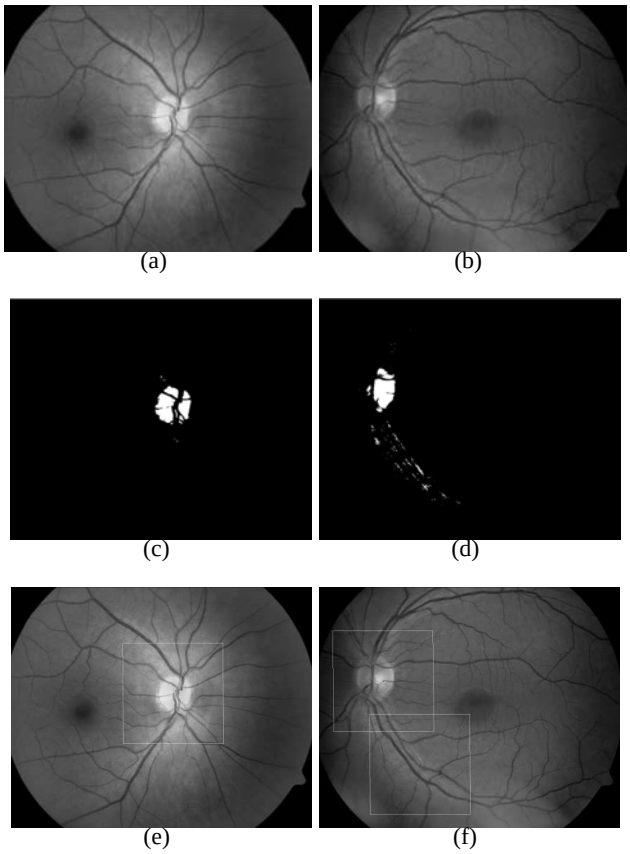

Fig 1: Top: original digital retinal images. Middle: selected points (highest 1% gray levels) which the clustering algorithm is applied to. Bottom: the regions of interest computed by means of the clustering algorithm when applied to images 1(a) and 1(b).

Figure 1 shows the points which the clustering algorithm is applied to. The regions of interest computed by means of this process are also depicted in this figure.

2.2 Correlation Filter

As depicted in Figure 1(f), several regions of interest might be computed by means of the clustering algorithm because of bright areas in the retinal images. A correlation filter is applied to each region in order to locate the true region where the optic disk is situated.

The optic disk consists of a high intensity near-circular disk, with a roughly centrally band of low intensity vessels. Due to this fact, the template consists of a Laplacian of Gaussian with a vertical channel in the middle to correspond to the major vessel band. This correlation filter is shown in Figure 2, where all commented features of the filter are depicted.

The template is correlated with the intensity component of the retinal image. We use the full Pearson-

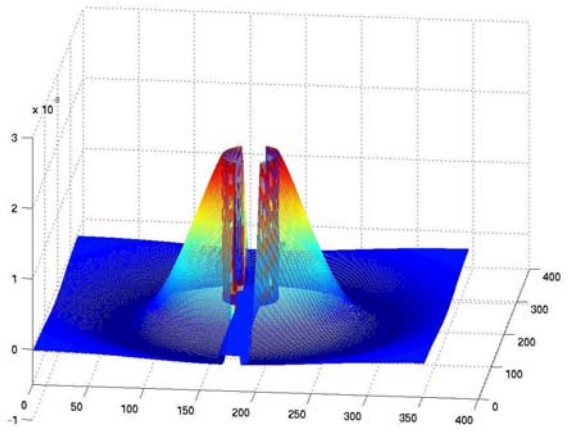

Fig 2: The correlation filter, where the template consists of a Laplacian of Gaussian with a vertical channel in the middle corresponding to the major vessel band

R correlation to take variations in mean, intensity and contrast into account, as defined in Equation 3.

$$C_{i,j} = \frac{\sum_{x,y}(f(x,y) - \bar{f}(x,y))(w(x-i,y-j) - \bar{w})}{\sum_{x,y}(f(x,y) - \bar{f}(x,y))^2 \sum_{x,y}(w(x-i,y-j) - \bar{w})^2} \quad (3)$$

where $\bar{w}$ is the mean value of the template and $\bar{f}$ is the mean value of the area covered by w.

The region of interest containing the optic disk is defined as $n \times m$ rectangle whose center is the point with the higher response computed by means of the correlation filter. Figure 3 shows the final region of interest of a retinal image in which the clustering algorithm computed two different regions.

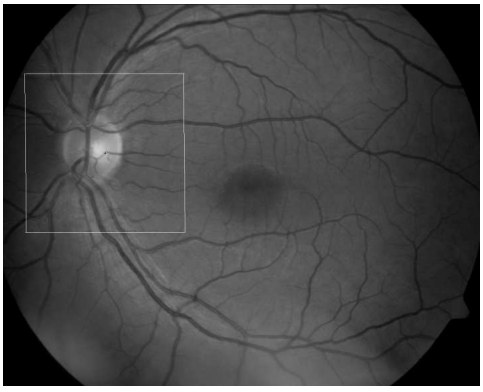

Fig 3: Region of interest defined as $n \times m$ rectangle whose center is the point with the higher response computed by the correlation filter applied to the regions shown in Figure 1(f), showing only the right region where the optic disk is located in, and discarding the wrong region.

3 Optic Disk Segmentation

Once the region containing the optic disk is computed, the extraction of the optic disk is performed by means of a deformable model. Deformable models or snakes were introduced by Kass et al. [9], and since then they have widely studied and many different models have appeared [10–12] among others, resulting in a invaluable tool for the medical images analysis [11, 13–15]. In this work the deformable model used in the segmentation performs like the proposed by Hu et al. [16], but with some improvements to get a better segmentation of the optic disk nerve head.

Firstly, will briefly introduce Hu's work, in order to explain later the improvements applied to this first proposal.

3.1 Hu's Circular Model

The deformable model from Hu et al. [16] works by combining two models: a global model and a local model. The global model is a circle with center **c** and radius r, and is used to get a rough fitting to the border of the optic disk. The local model is defined by the center **c** and evenly spaced radial spokes, and direction vector $s_i = [\cos(\theta_i), \sin(\theta_i)]$. The model is defined by distances m_i from **c** along each spoke. The local model has a corresponding global model with radius $r = \overline{m}_i$, the local model's mean radial displacement.

The force f which guides the process has two components: an internal force f^{int} and an external force f^{ext}. The forces work along the radial spokes. The external force drags the model toward the attractor points. The internal force limits model deformation using two components: global force, which pulls the model toward the global shape, and the local force, which smoothes the model by penalizing differences in deformation between neighboring spokes.

For a better fitting, three modifications were introduced to this model, following the work from Lowell et all. [5, 17, 18]. For the sake of brevity, and since this step is perfectly covered by referenced literature, only results will be included in this work.

4 Macula And Fovea Detection

The fovea is a small depression on the fundus (in Figure 4 the macula is marked by an arrow). It is the darkest part in most of the retinal images, while it is not obvious in some images due to high illumination or being covered by the lesions. Its geometrical relation to other structures is employed to locate the fovea robustly. The method performs in two steps: firstly, a candidate area containing the macula is obtained. Then the macula size and position is located within this search area by means of a matched filter.

Fig 4: Location of the macula in the eye fundus retinography marked by a dark arrow. It is clear the position of the macula in a region without retinal vessels and between main vessels, which compose the two branches of the main vessel arc.

4.1 Macula Candidate Region Selection

The candidate region of fovea is defined as an area of circle. Its center is located approximately at 2 disk diameter away from the disk center and its size is the same than the optic disk. Because the fovea is located about 2 times optic disk size temporal to the optic disk in the retinal images [19], the candidate region is such defined in order to ensure that the fovea is within the region.

The definition of the foveal candidate area is as follows: firstly, creases from the image are obtained [20], as shown in Figure 5, where a digital retinal image (Figure 5(a)) an its extracted creases (Figure 5(b)) are depicted. Then, by means of a filtering process, all creases except the creases from the main vessels are removed (main creases are marked as c_1 and c_2 in Figure 6), because fovea will always be within the area determined by this creases. The filtering process consists on taking only the two longest creases, which will always belong to the the main vessels arc creases.

Then an arc is drawn with a radius of two times optic disk diameter, and points A and B are taken, from the intersection of this arc and the creases. The straight line r_1 which passes through both this points is considered, and then the new straight line r_2 which goes from the optic disk center passing by the midpoint of r_1 is drawn. Finally, the point C where r_2 intersects $\widehat{AB}$ is defined as the center of the candidate area. Although the size of the macula is about the optic disk, the size of the candidate area is again two times the optic disk, ensuring that way that the macula will always be within the search region (Figure 6 shows an schematic representation of these procedure).

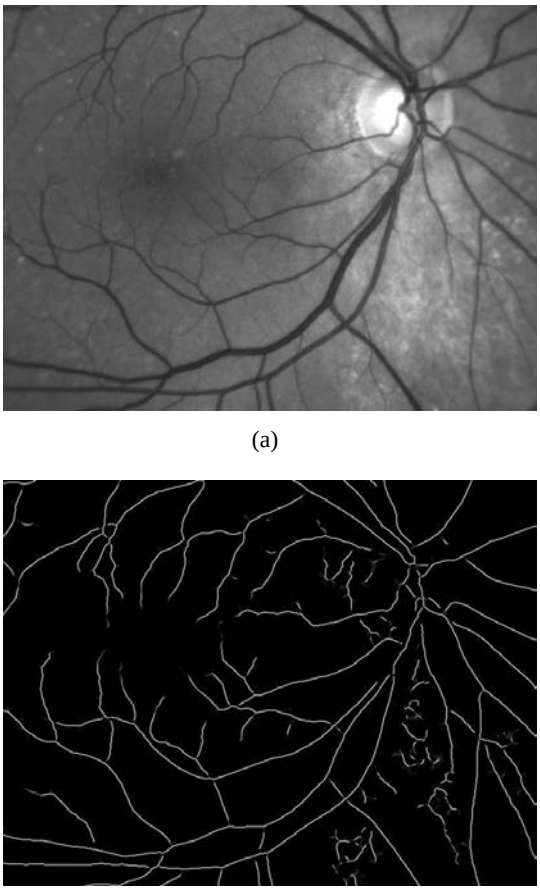

(a)

(b)

Fig 5: Digital retinal image (top) and the all the creases extracted from this image (bottom).

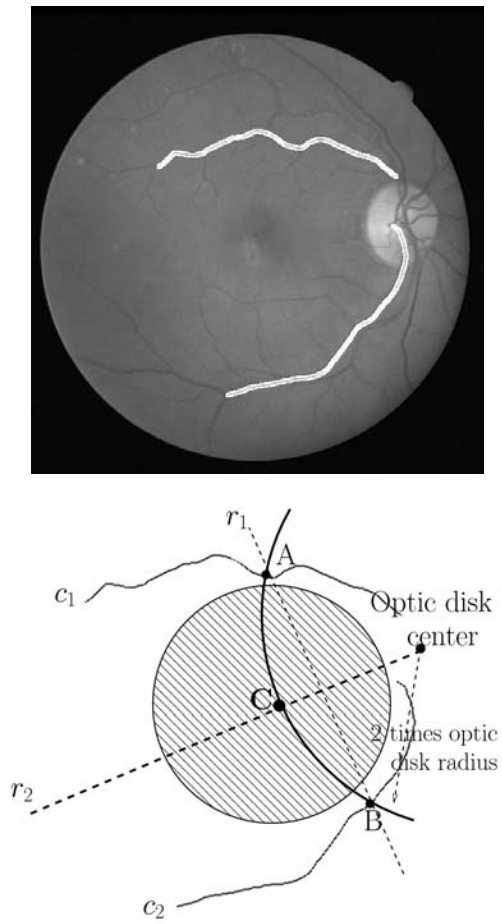

Fig 6: Computation of the candidate foveal region. Top: digital retinal angiography with creases of the arch vessel in white (oversized for better visualization). Middle: scheme of the foveal candidate region composition from the optic disk (center and radius) and creases of the vessel arc (candidate region is marked as a shaded circular area). Bottom: original retinography with the scheme superimposed, with the macula always laying inside the foveal candidate area.

4.2 Macula Segmentation

Once the candidate area containing the macula have been obtained, a correlation filter is applied to the region in order to locate the macula and so the fovea.

As stated before, the fovea is a spot located in the center of the macula, and responsible for sharp central vision. The macula macula is a commonly visible as a hazy dark area. To locate this dark area, a matched filter which consists of a Laplacian of Gaussian is used. The correlation filter is shown in Figure 7. The fovea will be located at the position where the response of the filter is maximum.

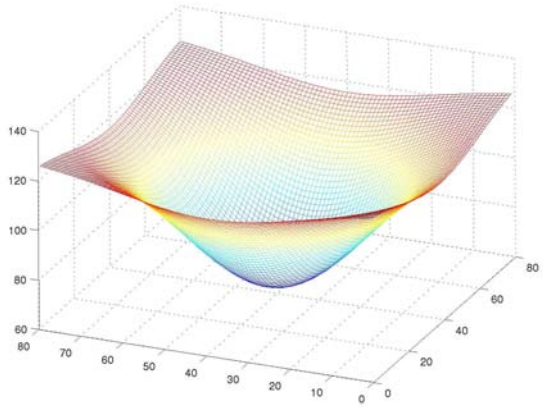

Fig 7: The correlation filter to locate the macula, where the template consists of a Laplacian of Gaussian

The template is correlated with the intensity component of the retinal image. We use the full Pearson-R correlation to take variations in mean, intensity and contrast into account, as defined in Equation 3. The size of the filter is taken the same as the optic disk size, since the diameter of the macula is about the same as the diameter of the optic disk [19].

The region of interest containing the macula is defined as $n \times m$ rectangle whose center is the point with the higher response computed by means of the correlation filter. Figure 8 shows the result obtained in the macula segmentation process. Macula is marked as a circle about the center of the image, while fovea is marked as a cross in its center (optic disk segmentation result is also included, with its center marked as a red cross).

5 Results

To test the accuracy of the localization and segmentation algorithms described below, a set of 135 images where used as the benchmark. Images were acquired in different centers of the Complejo Hospitalario Universitario de Santiago de Compostela (CHUS), all of

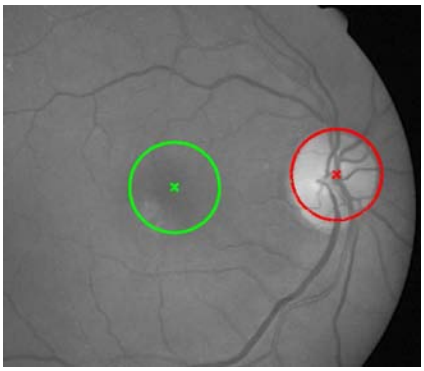

Fig 8: Result obtained from the macula segmentation process using the correlation matched filter in image from Figure 6.

	Localization		
	Good	**Fair**	**Poor**
Number images %	132	3	0
(Clinician 1 vs Clinician 2)	97.78	2.22	0.00
	100.00%		0.00%
Number images %	128	6	1
(Aut. vs Clinician 1)	94.82	4.44	0.74
	99.26%		0.74%
Number images %	126	8	1
(Aut. vs Clinician 2)	93.33	5.93	0.74
	99.26%		0.74%

Table 1: Results obtained in each stage (localization and segmentation) of the process compared with each of the clinician's manual results (Aut. vs Clinician 1 and 2), as well as the clinician's inter-variability (Clinician 1 vs Clinician 2). Three quantitative categories were defined (good, fair, poor), with disparities one, two or more, respectively, computed using equation 4

them with a Cannon CR6-45NM Non-Mydriatic Retinal Camera, with a 768×576 pixel resolution. Although the camera originally captures color images, a conversion to gray-level images (with 256 gray levels) was performed prior to the application of the algorithms, since color does not provide any useful information.

Validation of the algorithms was performed by two expert clinicians, one from the CHUS and the other from the Hospital Provincial de Conxo, who analyzed the output of the techniques to set its accuracy.

To validate our experiments, the clinicians segmented manually the optic nerve head (marking its center) and macula (marking the fovea) from the test images, and these results were compared with the results obtained by the application of the process described in the preceding sections. Results for the first stage of the algorithm are included in [17, 18], so they will not be presented here.

Results from the comparisons for the macula localization are shown in Table 1, where three categories were defined (good, fair, poor), function of the difference between the results obtained by clinicians and automatic results, as well as for the clinician's inter-variability.

For each of this comparisons (clinician vs clinician and automatic vs clinician) one group of rows can be found in the table: one row with the total amount of images in each category, the percentage of images in each category in another row, and the total percentage of images in the good-fair category. This discrepancy for image j was computed using equation 4 [1].

$$\delta^i = \sum_{i=1}^{9} \frac{\left|\mathbf{C}_j - \mathbf{C}'_j\right|}{9} \tag{4}$$

with $\mathbf{C}_j$ representing the automatic segmentation of the macula, $\mathbf{C}'_j$ representing the manually segmented macula rim and the summation over 8 points evenly spaced (one each $\pi/4\,rad$) plus the fovea point, taken from each of the obtained macula rim estimations.

Analyzing results shown in Table 1, macula localization gives an average effectiveness of 99.26%, which is a very good percentage, similar to the results for the inter-clinician comparison. The image giving a poor result is depicted in Figure 9. In that image the difference between the result obtained manually by the clinician was not so similar to the one obtained with our method because of the blurriness of the macula, giving raise to the poor result presented.

Fig 9: Image showing poor result for the macula localization. Macula manually obtained by the clinician is represented by the red circle, and macula obtained by our method is represented by the green circle.

To illustrate these results, Figure 10 depicts several result images from the localization and segmentation of the optic disk (rim and center), macula and fovea.

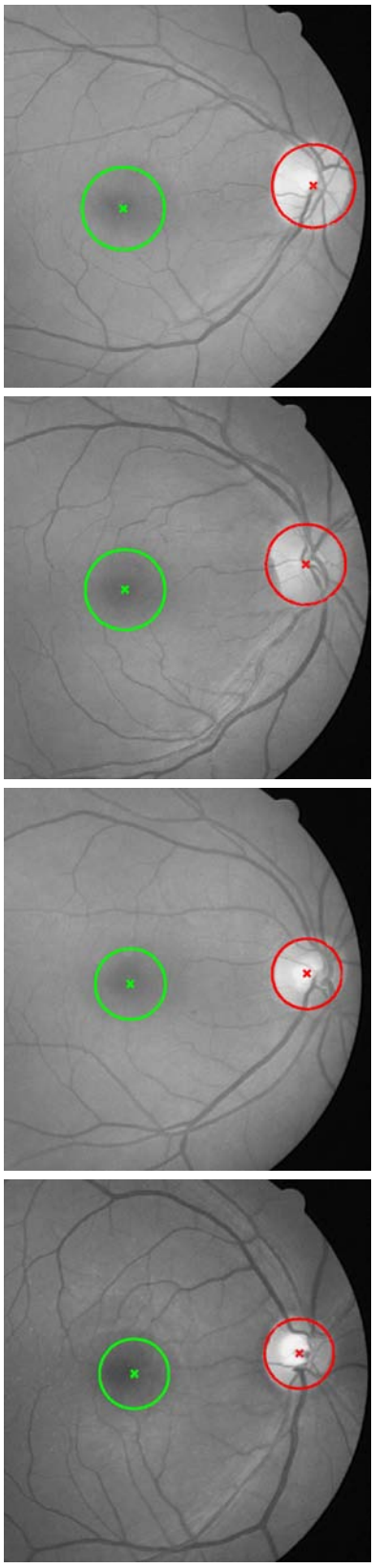

Fig 10: Result images showing the optic disk with its center (red circle and red cross, respectively) and macula with the fovea (green circle and green cross, respectively) in several images.

6 Conclusions

In this work an algorithm for the precise localization and segmentation of the optic disc nerve head and localization of the macula has been presented. The optic disk localization algorithm performs in two stages: in the first, the region of interest where the optic disc is located is obtained by combining a clustering process with a posterior correlation procedure.The size of the central channel (corresponding to the main optic disc vessel) has been estimated, with a mean size in the test set of 20 pixels, which is also the size of this area in the correlation kernel.

By other side, the size of this filter has been calculated for the set of images in the test set, getting sizes from $130px$ to $220px$. Since the filter must have at least the size of the bigger optic disc, commented results have been obtained with a kernel of $221 \times 221px$, which have performed well for the whole set of images. In the second stage, the located optic disc is segmented through a deformable model, proposed by Lowell et al. and which we re-implemented with very good results (successful percentages of 93.33% and 94.82 compared with manual results from two expert clinicians [17, 18]).

For the macula and fovea localization, the morphological properties of the eye has been used. A candidate region for the localization of the macula is computed two optic disk diameters away from the optic disk center obtained in the previous stages. Once located this area, a search is performed through a correlation procedure, with a Gaussian kernel with the size determined by the optic disk size, since the macula is about the size of the optic disk. Obtained results show a successful percentage 99.25% in a test set of 135 digital retinal images.

The whole process has taken an average time of 2.2 seconds in the experiment performed, with a set of 135 different digital retinal images. Times for each of the stages are included in Table 2.

Stage	Average time (seconds)
Localization stage	1.1
Segmentation stage	0.3
Macula localization stage	0.8

Table 2: Times obtained for each of the different stages of the macula segmentation and fovea localization algorithm

In the future work we will test the algorithm with a wider set of images, trying to evaluate the effect of images with diseases like diabetic retinopathy in the results. By other side, we are working on several improvements to both the proposed algorithms. By one side, a better fitting to the optic disk which will also

improve the detection of the macula, since both diameters are related. By other side, obtaining a better segmentation of the macula by a multiscale approximation.

Acknowledgements: This paper has been partly funded by the Xunta de Galicia through the grant contracts PGIDT04PXIC10501PN and PGIDIT06TIC10502PR.

References

[1] Goldbaum M., Moezzi S., Taylor A., Chatterjee S., Boyd J., Hunter E., and Jain R. Automated Diagnosis and Image Understanding with Object Extraction, Object Classification, and Inferencing in Retinal Images. In *Proceedings of the International Conference on Image Processing*, vol. 3, 1996.

[2] Pinz A., Bernögger S., Datlinger P., and Kruger A. Mapping the human retina. *IEEE Transactions on Medical Imaging*, vol. 17(4), 1998, pp. 606–619.

[3] Lalonde M., Beaulieu M., and Gagnon L. Fast and robust optic disk detection using pyramidal decomposition and Hausdorff–based template matching. *IEEE Transaction on Medical Imaging*, vol. 20, 2001, pp. 1193–1200.

[4] Mendels F., C. H., and J.P. T. Identification of the optic disk boundary in retinal images using active contours. *Proceedings of the Irish Machine Vision and Image Processing Conference*, 1999, pp. 103–115.

[5] Lowell J., Hunter A., Steel D., Basu A., Ryder R., Fletcher E., and Kennedy L. Optic nerve head segmentation. *IEEE Transactions on medical Imaging*, vol. 23, 2004, pp. 256–264.

[6] Chanwimluang T. and Fan G. An efficient algorithm for extraction of anatomical structures in retinal images. *IEEE International Conference on Image Processing*, vol. 23, 2004, pp. 1093–1096.

[7] Sinthanayothin C., Boyce J., Cook H., and Williamson T. Automated localisation of the optic disc, fovea and retinal blood vessels from digital colour fundus images. *British Journal of Ophthalmology*, vol. 83, 1999, pp. 902–910.

[8] Li H. and Chutatape O. Automated Feature Extraction in Color Retinal Images by a Model Based Approach. *IEEE Transactions on Medical Imaging*, vol. 51(2), 2004, pp. 246–254.

[9] Kass M., Witkin A., and Terzopoulos D. Active Contour Models. *International Journal of Computer Vision*, vol. 1(2), 1988, pp. 321–331.

[10] Bro-Nielsen M. Active Nets and Cubes, 1994.

[11] Cootes T.F., A. Hill C.J.T., and Haslam J. Use of active shape models for locating structures in medical images. *Image and Vision Computing*, vol. 12(6), 1994, pp. 355–365.

[12] Giraldi G., Strauss E., and Oliveira A. Dual-T-Snakes model for medical imaging segmentation. vol. 24(7), 2003, pp. 993–1003.

[13] Pardo X.M., Carreira M.J., Mosquera A., and Cabello D. A snake for CT image segmentation integrating region and edge information. *Image and Vision Computing*, vol. 19(7), 2001, pp. 461–475.

[14] Hang X., Greenberg N.L., and Thomas J.D. A geometric deformable model for echocardiographic image segmentation. *Computers in Cardiology*, (4), 2002, pp. 77–80.

[15] Yan P. and Kassim A.A. Medical image segmentation with minimal path deformable models. In *International Conference on Image Processing, 2004. ICIP '04*, vol. 4, 2004.

[16] Hu Y.L., Rogers W.L., Coast D.A., Kramer C.M., and Reicheck N. Vessel boundary extraction based on a global and local deformable physical model with variable stiffness. *Magnetic Resonance Imaging*, vol. 16, 1998, pp. 943–951.

[17] Mariño C., Barreira N., Penedo M.G., Ortas M., Pérez-Urria A., Doncel J.L., and González F. Optic disc segmentation using a matching filter and a deformable model. In *International Conferences WSEAS on Applied Computer Science*, vol. 1, 2006.

[18] Mariño C., Barreira N., Penedo M.G., Ortas M., Doncel J.L., and Gómez-Ulla F. Two stages optic disc segmentation in digital retinal images. *WSEAS Transactions on Information Science and Applications*, vol. 4(4), 2007, pp. 771–778.

[19] Larsen H.W. *The Ocular Fundus: A Color Atlas*. Munksgaard, 1976.

[20] Mariño C., Penedo M.G., Penas M., Carreira M.J., and González F. Personal authentication using digital retinal images. *Pattern Analysis and Applications*, (9), 2006, pp. 21–33.